Soft Matter

Modeling collagen fibril degradation as a function of matrix microarchitecture

Journal:	*Soft Matter*
Manuscript ID	SM-ART-08-2024-000971.R1
Article Type:	Paper
Date Submitted by the Author:	31-Oct-2024
Complete List of Authors:	Debnath, Bhanjan; San Diego State University, Mechanical Engineering Narasimhan, Badri Narayanan; University of California San Diego Fraley, Stephanie; University of California San Diego, Bioengineering; University of California San Diego, Rangamani, Padmini; University of California San Diego, Department of Pharmacology

Modeling collagen fibril degradation as a function of matrix microarchitecture

Bhanjan **Debnath**[1], Badri Narayanan **Narasimhan**[2], Stephanie I **Fraley**[*2], and Padmini **Rangamani** [*1,3]

[1]*Department of Mechanical and Aerospace Engineering, University of California San Diego, CA 92093, USA*

[2]*Department of Bioengineering, University of California San Diego, CA 92093, USA*

[3]*Department of Pharmacology, School of Medicine, University of California San Diego, CA 92093, USA*

Abstract

Collagenolytic degradation is a process fundamental to tissue remodeling. The microarchitecture of collagen fibril networks changes during development, aging, and disease. Such changes to microarchitecture are often accompanied by changes in matrix degradability. In a matrix, the pore size and fibril characteristics like length, diameter, number, orientation, and curvature are the major variables that define the microarchitecture. *In vitro*, collagen matrices of the same concentration but different microarchitectures also vary in degradation rate. How do different microarchitectures affect matrix degradation? To answer this question, we developed a computational model of collagen degradation. We first developed a lattice model that describes collagen degradation at the scale of a single fibril. We then extended this model to investigate the

[*]To whom correspondence must be addressed: sifraley@ucsd.edu and prangamani@ucsd.edu

role of microarchitecture using Brownian dynamics simulation of enzymes in a multi-fibril three dimensional matrix to predict its degradability. Our simulations predict that the distribution of enzymes around the fibrils is non-uniform and depends on the microarchitecture of the matrix. This non-uniformity in enzyme distribution can lead to different extents of degradability for matrices of different microarchitectures. Our simulations predict that for the same enzyme concentration and collagen concentration, a matrix with thicker fibrils degrades more than that with thinner fibrils. Our model predictions were tested using *in vitro* experiments with synthesized collagen gels of different microarchitectures. Experiments showed that indeed degradation of collagen depends on the matrix architecture and fibril thickness. In summary, our study shows that the microarchitecture of the collagen matrix is an important determinant of its degradability.

1 Introduction

Collagen is the most abundant protein present in tissues. Enzymatic degradation of collagen is an important process in both physiological and pathological conditions[1,2]. For instance, an imbalance between collagen degradation and production can lead to increased collagen accumulation resulting in fibrosis[3,4]. Such fibrotic environments have been associated with an impaired degradative environment[4]. Studies have shown that the microarchitecture of collagen in the fibrotic extracellular matrix (ECM) is substantially different from the healthy tissues and they show higher resistance to degradation[5,6]. As another example, cancer-associated fibroblasts in the tumor microenvironment secrete collagen and continuously remodel their matrix. This abnormal remodeling can lead to the cancerous microenvironment possessing a higher density of collagen and very different microarchitecture than a healthy ECM[7]. A body of work argues that alterations in collagen degradation can result in metastasis[8,9], and suggests possible connections between the matrix microarchitecture and its degradability[10–13].

However, the role of matrix microarchitecture in determining the degradability at the cellular length scale remains an open question. Here, we used multi-scale modeling and *in vitro* experiments to investigate possible mechanisms of matrix degradation at this length scale.

Most models of collagen gel degradation use Michaelis-Menten kinetics to model the collagenase activity and show good agreement with experiments in predicting the rate of total mass loss[14–17]. These models cannot address the connection between the microarchitecture and degradation because of their continuum structure. Another class of models have treated collagen fibril as a thin filament of negligible thickness (diameter $\sim 10-20$ nm) and proposed a degradation mechanism of one filament based on movements of a few collagenase molecules over the filament surface[18,19]. However, many experimental findings have reported that the collagen fibrils in a matrix are significantly thicker (diameter in the range $\sim 0.1-0.5\,\mu$m) than the value used in these models[11,20–23]. Therefore, an open challenge in the field is to determine how a filament-scale model can be extended to a fibril-scale model, and subsequently, to a model where multiple fibrils are interacting with many collagenase molecules in a three-dimensional matrix.

In this work, we investigated how matrix microarchitecture can affect its degradability. We developed a fibril-scale model using lattice-based approach to predict the degradation of single fibril. To predict degradation of multiple fibrils by many enzyme molecules in a matrix, we used Brownian dynamics to capture the enzyme distribution surrounding the fibrils in a three-dimensional matrix environment. We then combined the fibril-scale model with the enzyme distribution obtained from the Brownian dynamics simulations to predict the degradation of collagen matrices. Our model predicted that differences in the microarchitecture between two matrices of same collagen density can lead to different extents of degradation. Additionally, we predicted that fibril thickness can be an important determinant of degradation. We tested this prediction against *in vitro* experiments using collagen gels of different architectures, which showed that indeed, fibril degradation depends on the matrix microarchitecture. Thus our study

may provide new insights for understanding matrix alterations associated with disease and may influence the development of matrix targeted therapeutics, biomaterials and controlled drug delivery[2,24,25].

2 Methods

In this section, we describe the details of the single fibril model, Brownian dynamics (BD) simulations, and experimental methods. We elaborate on each step of the model development and justify the assumptions based on previous experimental observations. The notation and symbols used in this work are shown in Table 1.

2.1 Model development for the degradation of single fibril

We consider a single collagen fibril of mean diameter d_f and mean length ℓ_f. This fibril consists of a staggered arrangement of the triple helix tropocollagen units as shown in Fig. 1a[26–29]. The enzymatic degradation of the fibril occurs in the presence of collagenases such as matrix metalloproteinases (MMP). These collagenases cleave the triple helix at a site that is at a distance ~ 67 nm (approx. 1/4 of the length of the triple helix) from the C-terminal of the tropocollagen unit (Fig. 1a)[30,31].

Previous experiments have reported that the collagenolytic degradation is a surface erosion process[14,32,33]. The minimum effective pore size inside a collagen fibril is a few multiples of the diameter of the tropocollagen, which is $d_{\mathrm{TC}} \sim 1.5$ nm[26]. This dimension is smaller than the size of the collagenase molecules which is in the range 50-120 kDa with a mean hydrodynamic diameter of $d_E \sim 10 - 20$ nm[34]. Based on the dimensions and following previous studies[14,32,33], we assume that the diffusion of MMPs through the pores of the fibril can be ignored, and we model the fibril degradation as a surface erosion process.

We treated the fibril surface as a series of lattice sites to model the surface erosion process. The loss of lattice sites effectively is a measure of degradation. However,

predicting the size of a degrading fibril from the extent of lattice sites lost during degradation is not straightforward. Here we followed a lumped modeling approach to link the average size of a fibril to the number of lattice sites.

To simulate the surface erosion of the fibril, we developed a lattice-based model. We divided the tropocollagen unit into lattice sites each of length d_m. Based on the number of amino acid residues at the cleavage site region[33], we set $d_m = 8$ nm. As the cleavage site is at a distance 1/4 of the length of the tropocollagen from its C-terminal, we assumed that there is one vulnerable site (V) per tropocollagen unit, and we treat the rest of the lattice sites as regular sites (R) (see Fig. 1a). With these dimensions, we developed a relation between the size of a fibril and the number of lattice sites available at its surface. To obtain the total number of lattice sites on the fibril surface, we next estimate the number of tropocollagen units on that surface. At any given time t, the number of tropocollagen units available for collagenolysis at the fibril surface is

$$N^s_{\mathrm{TC}} = \frac{\pi\, d_f\, \ell_f}{d_{\mathrm{TC}}\,(\ell_{\mathrm{TC}} + 0.54\,\mathrm{D})}, \tag{1}$$

where ℓ_{TC} is the length of the tropocollagen unit and (0.54 D) is the gap between two tropocollagen units (D $\sim$ 67 nm) (see Fig. 1a). Thus, the total number of sites N^s at time t exposed at the fibril surface is

$$N^s = \frac{\ell_{\mathrm{TC}}}{d_m}\, N^s_{\mathrm{TC}} = \frac{\ell_{\mathrm{TC}}}{d_m}\, \frac{\pi\, d_f\, \ell_f}{d_{\mathrm{TC}}\,(\ell_{\mathrm{TC}} + 0.54\,\mathrm{D})}. \tag{2}$$

Eqn (2) highlights the relationship between the total number of sites available for degradation and the size of the fibril. The number of vulnerable sites N^s_V exposed at the surface is the same as N^s_{TC} because one tropocollagen unit contains one vulnerable site, i.e., $N^s_V = N^s_{\mathrm{TC}}$. Therefore the remaining $N^s_R = (N^s - N^s_V)$ are regular sites. Using eqn (2), we can estimate either ℓ_f or d_f. As the vulnerable sites are not aligned at the same plane inside the fibril (see Fig. 1a) and the collagenolytic degradation is a surface erosion process, we treat ℓ_f as a constant and predict d_f from eqn (2).

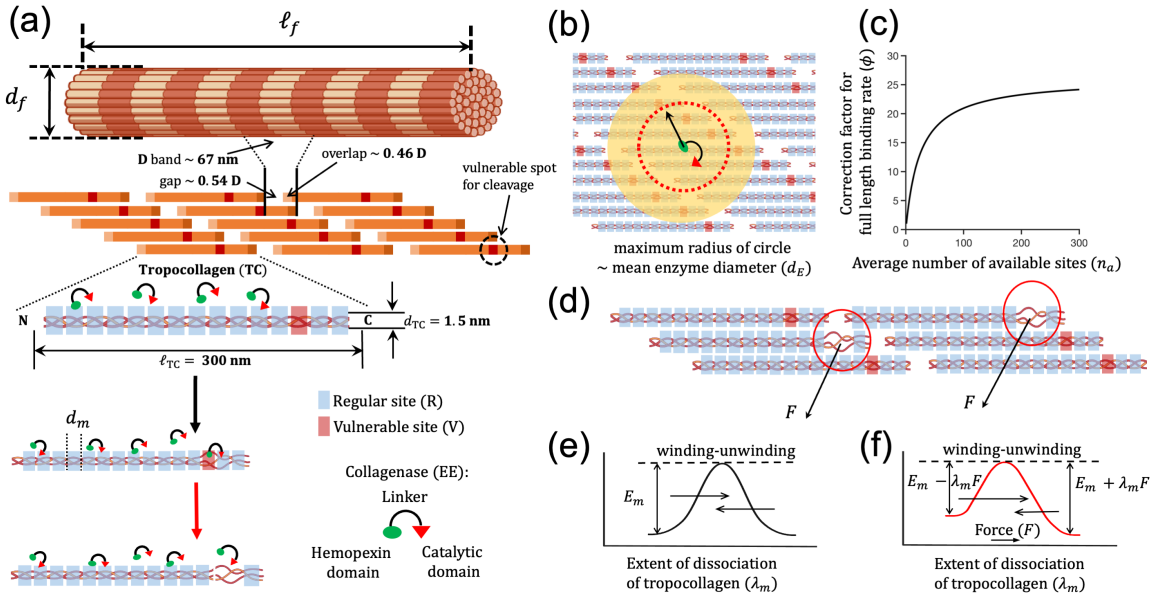

Figure 1: Modeling single fibril degradation. (a) Overview of the hierarchical organization of a collagen fibril and the degradation mechanism. We divide the tropocollagen unit into lattice sites (regular and vulnerable sites). The structure of the collagenase enzymes has two domains. (b) When one domain of the enzyme is bound to one lattice site, the other domain has access to only the neighboring unoccupied sites inside the red-dashed circle, whose radius is equivalent to the hydrodynamic mean diameter (d_E) of the enzyme. (c) To incorporate this effect in the intrinsic rates of the full-length binding (when both domains of an enzyme are bound to the lattice sites)/hopping kinetics, we propose a correction factor (ϕ) as a function of available sites (n_a). (d) We propose that the enzyme-induced irreversible unwinding of the vulnerable sites induces a force, which affects the unwinding rate of the neighboring regular sites. The symmetric (e) and asymmetric (f) energy barriers for the winding-unwinding process of a lattice site.

As mentioned earlier, using Eqns 1 and 2, we will predict the average diameter of the fibril. It may happen that degradation at all points on a fibril surface do not occur at the same rate. This inhomogeneity can lead to spatial variations in the diameter and the shape of the fibril cross-section along the length of the fibril. These spatial variations cannot be captured using Eqns 1 and 2, as they represent a lumped system.

Table 1: Notation and list of symbols.

Notation	Description
d_f	mean diameter of a fibril
ℓ_f	mean length of a fibril
d_{TC}	diameter of the tropocollagen unit
ℓ_{TC}	length of the tropocollagen unit
d_E	mean hydrodynamic diameter of an enzyme
d_m	length of one lattice site
R	regular site
V	vulnerable site
EE	enzyme with two domains
E_*E_* class of symbols	enzyme partially (E_*E) or, fully bound (E_*E_*)
	to regular ($* = R$) or, vulnerable ($* = V$) sites
k_*^* class of symbols	different rate constants
N^s	total sites exposed on the fibril surface
N_R^s	number of regular sites exposed on the fibril surface
N_V^s	number of vulnerable sites exposed on the fibril surface
N_{EE}	number of free enzymes
$N_{E_*E_*}^s$ class of symbols	number of enzymes partially (or, fully) bound
	to regular (or, vulnerable) sites
ϕ	correction factor for intrinsic rates of full-length binding kinetics
n_a	number of available lattice sites per enzymes at partially-bound state
E_m	energy required to cross the symmetric energy barrier
λ_m	extent of dissociation at the unwound state
F	average force experienced by the lattice sites
γ	surface energy per unit area
τ_c	characteristic time associated with force dependent kinetics
τ_e	time for disentanglement of tropocollagen chains
l_p	nominal length scale
N_e^0	number of enzymes surrounding a fibril
$(N_e^0)_{total}$	total number of enzymes in the simulation box
D_e	diffusivity of enzymes
ϕ_f	volume fraction of fibrils
n_f	number of fibrils in the simulation box
A_f^0	initial surface area of a fibril
$(A_f^0)_{total}$	initial total surface area of all fibrils

Development of a reaction scheme to model the loss of lattice sites on a fibril

Previous experimental findings have shown that the MMP class proteinases (for example, MMP1) hydrolyze the peptide bonds at the vulnerable site of the collagen type I[30,31]. Researchers hypothesized that the enzyme destabilizes the structure of the tropocollagen, and induces local unwinding around the vulnerable site before cleavage[30,33,35]. Using the hypotheses of Chung et al.[30] and Perumal et al.[33], and making the following assumptions, we propose a reaction scheme for enzyme kinetics (see Fig. 1a and the supplementary information (SI) section SI1 (Fig. S1)).

1. There are two types of lattice sites on the collagen surface: regular site (R) and vulnerable site (V). The MMP has two domains: Hemopexin (Hpx) domain and Catalytic (Cat) domain connected by a linker[36,37]. Manka et al.[38] had shown a strict requirement of both domains to be linked together for efficient enzyme-collagen binding and collagenolysis.

2. Following Manka et al.[38], we assume that the collagenase molecule has two domains, denoted by EE. Using these domains, the enzyme binds to the lattice sites via adsorption-desorption mechanism and hops on the sites. For the sake of simplicity, we assume that these two domains are equivalent and are of the same size.

3. First, using any one domain, the enzyme binds to a single site, in what is denoted as 'reversible partial binding'. This type of binding can result in two possible reactions.

$$EE + R \underset{k_-^1}{\overset{k_+^1}{\rightleftharpoons}} E_R E \qquad\qquad EE + V \underset{k_-^2}{\overset{k_+^2}{\rightleftharpoons}} E_V E \tag{3}$$

For the reversible partial binding (eqn (3)), we implement the protein adsorption-desorption kinetics[39,40] (see a short note on adsorption kinetics in section SI2).

4. When one domain of the enzyme is bound to one site, the other domain can also bind to another site. When both domains of an enzyme are in bound state, we term this state as 'full-length binding'. The enzyme molecule can jump or change track via hopping[18,19]. It hops on the regular sites via reversible binding-unbinding of one domain to a regular site while its other domain remains bound to another regular site.

$$E_R E \, + \, R \underset{k_-^3}{\overset{k_+^3}{\rightleftharpoons}} E_R E_R \tag{4}$$

5. Once the enzyme reaches a vulnerable site with both domains in the bound state, hopping stops, and is followed by enzyme-induced unwinding and the formation of product sites. These product sites are no longer available for binding new enzyme molecules.

$$E_V E \, + \, R \xrightarrow{k_+^4} E_V E_R \qquad\qquad E_R E \, + \, V \xrightarrow{k_+^5} E_V E_R \tag{5}$$

$$\text{Unwinding}: \quad E_V E_R \xrightarrow{k_+^w} (E_V E_R)^* \tag{6}$$

$$\text{Product formation}: \quad (E_V E_R)^* \xrightarrow{k_+^c} P + EE \tag{7}$$

For the cases of full-length binding/hopping represented by eqn (4)-(5), the forward reactions cannot be treated as second order kinetics because once one domain of an enzyme is bound to one site, its other domain does not have accessibility to all available lattice sites on the surface (see Fig. 1b). The unbound domain of the enzyme can find another lattice site for binding within a searching circle whose radius is equivalent to d_E (the mean hydrodynamic diameter of the enzyme). To correct the intrinsic rates of full-length binding kinetics, we multiply the rates with a correction factor ϕ. We propose a phenomenological function for ϕ as (Fig. 1c)

$$\phi \approx \frac{\pi \, (d_E)^2}{d_m \, d_{\mathrm{TC}}} \, \frac{n_a}{c_1 + n_a}, \tag{8}$$

where n_a is the number of available sites on the fibril surface. See section SI3 for more details of ϕ and section SI4 for the system of ODEs representing eqn (3)-(7).

The enzyme-induced permanent unwinding followed by cleavage happens only at the exposed vulnerable sites in collagenolysis. However, it is not clear how the fibril will lose other exposed regular sites at the surface due to the cleavage events so that the new surfaces can be easily accessible to the enzymes for further degradation[18,19,30,33,41]. Hence, we propose that the enzyme-induced permanent unwinding at the vulnerable sites generates a force which assists the removal of more regular sites exposed at the surface. We use the nonequilibrium rate-process theory of Eyring[42–44] and propose a new rate-term $\Re$ related to the force-dependent kinetics in an *ad hoc* manner in the system of ODEs. We briefly describe $\Re$ below.

As a result of thermal fluctuations, the lattice sites can be in any state between the triple helical and (temporary) unwound configurations[33]. If the rates of transition from the triple helical state to the unwound state and *vice-versa* are equal, there is no net change in the tropocollagen units in absence of enzymes. We hypothesize that enzyme-induced permanent unwinding that leads to cleavage generates a local stress (Fig. 1d). This mechanism is similar to the enzyme pulling chew-digest mechanism proposed by Eckhard et al.[45]. As a consequence, the other regular sites at the surface experience an external force which affects the kinetics by increasing their net rate of unwinding (Fig. 1e,f). This force can cause the slippage of chains, resulting in detachment from the surface[46,47].

To incorporate the force-dependent kinetics, we add a new term $\Re = k_R\, N_R^s$ in an *ad hoc* manner to the system of ODEs (see section SI4 for the system of ODEs). Here k_R is the net rate of flow over the energy barrier towards force assisted unwinding (Fig. 1e,f). We propose the following expression for k_R[48,49]

$$k_R \;=\; \frac{k_B T}{h}\left[\exp\left(\frac{-(E_m - \lambda_m F)}{k_B T}\right) - \exp\left(\frac{-(E_m + \lambda_m F)}{k_B T}\right)\right], \tag{9}$$

where h is Planck constant, k_B is the Boltzmann constant, and T is the temperature.

Here, E_m is the energy required to cross the symmetric barrier (Fig. 1e), λ_m is the extent of dissociation in unwound state which is chosen as ~ 3.6 Å [33]. Here F is the average force experienced by the remaining lattice sites. This force changes the energy barrier of unwinding to be asymmetric (Fig. 1f). If $F = 0$, $k_R = 0$. Following a heuristic approach, the average force (per remaining lattice site) is

$$F \sim \frac{1}{N^s} \left(\gamma\, d_m\, k_+^c\, \tau_c\right) \left(2\, k_+^w\, N^s_{E_V E_R}\right) \tau_e, \tag{10}$$

where $\gamma \sim \frac{k_B T}{d_m d_{\mathrm{TC}}}$ is the surface energy per unit area[50,51], k_+^c and k_+^w are rate constants of cleavage and enzymatic unwinding, respectively, $N^s_{E_V E_R}$ is the number of enzymes at fully-bound state (one regular and one vulnerable sites), τ_c and τ_e are, respectively, a characteristic time and time required to form disentangled chains during detachment from the surface. See sections SI5 for more details of F, τ_c and τ_e, section SI6 for the reaction rate constants, and section SI7 for the initial conditions to solve the ODEs. We solved the system of ODEs using ODE23s in MATLAB (Mathworks, Natick, MA).

2.2 Brownian dynamics (BD) to estimate the enzyme distribution around fibrils in a matrix

We next set up a collagen matrix that consists of stationary non-overlapping cylindrical fibrils (Fig. 2a,b) for different fibril fractions. We modeled the enzymes as spheres with a diameter of 10 nm[34], and simulated their Brownian motion using overdamped Langevin dynamics[52]. We used MATLAB to set up the simulations. The fibrils and enzymes are inserted in the simulation box such that they do not overlap and are treated as hard particles. The fibrils are randomly inserted[53,54]. Periodic boundary conditions are applied in all three directions. For the sake of simplicity, all potential interactions among fibrils and molecules are neglected and the motion of the enzymes through the fibrous gel is simulated using Cichocki-Hinsen algorithm[55–57]. The free diffusivity D_e of the enzyme is set to 74×10^{-12} m^2/s[58]. The time step for simulations

is chosen $\Delta t_s = 10^{-6}$ s such that it is sufficiently small and the length increment in one time step is $\sqrt{D_e \, \Delta t_s} \sim \mathrm{O}(d_E)$, which is equivalent to the size of the enzyme $d_E \sim 10$ nm. In simulations and model predictions, all length dimensions are scaled by $l_p = 1$ µm, and the dimensions of the simulation box are chosen as $5\,l_p \times 5\,l_p \times 5\,l_p$. The entire codebase used in this work along with a readme file is available at `https://github.com/RangamaniLabUCSD/Collagen_matrix_degradation.git`.

For a length scale $l_p = 1$ µm and the diffusivity of the enzyme (collagenase) $D_e \sim 10^{-10}$ m^2/s[58], the time scale is of $\mathrm{O}(l_p^2/D_e) \sim \mathrm{O}(10^{-2})$ s. Hence the limit of instantaneous diffusion is valid in the long time limit for the chosen simulation box dimensions[14]. Based on this assumption, we proposed a hybrid framework (Fig. 2c). In this framework, we run the simulation for a period of time and then obtain the number of enzymes (N_e^0) surrounding the fibrils based on the shortest distances of enzymes from the fibrils (Fig. 2d). We use the values of N_e^0 to solve the single fibril model where the fibril-scale model considers the binding-unbinding and other types of interactions among the enzymes and fibrils through a set of reactions. Using this hybrid modeling framework, we predict the degradation of all individual fibrils, effectively the degradation of a matrix.

The number of simulation time steps must be such that the enzymes get enough time to distribute themselves inside the pores of the matrix. As the limit of instantaneous diffusion is valid, the time span would be 10^{-2} s to 1 s for a dimension of the simulation box 1 l_p to 10 l_p. Therefore, we chose the number of simulation time steps to obtain enzyme distribution around fibrils as 10^5 to 10^6, which is 10^{-1} s to 1 s. The enzyme distribution in this short time and in the long time limit would not differ, as BD simulations do not consider the attractive interaction potentials among enzymes and fibrils explicitly.

To perform the BD simulations, we chose an enzyme concentration ~ 2.5 µg/mL. For the simulation box volume $5\,l_p \times 5\,l_p \times 5\,l_p = 125\,l_p^3$, the weight of enzymes is 312.5×10^{-18} g. The molecular weight (M_w^e) of collagenase varies between 70-130 kDa. We have chosen $M_w^e \sim 120$ kDa[45]. For this chosen value, the estimate of total number

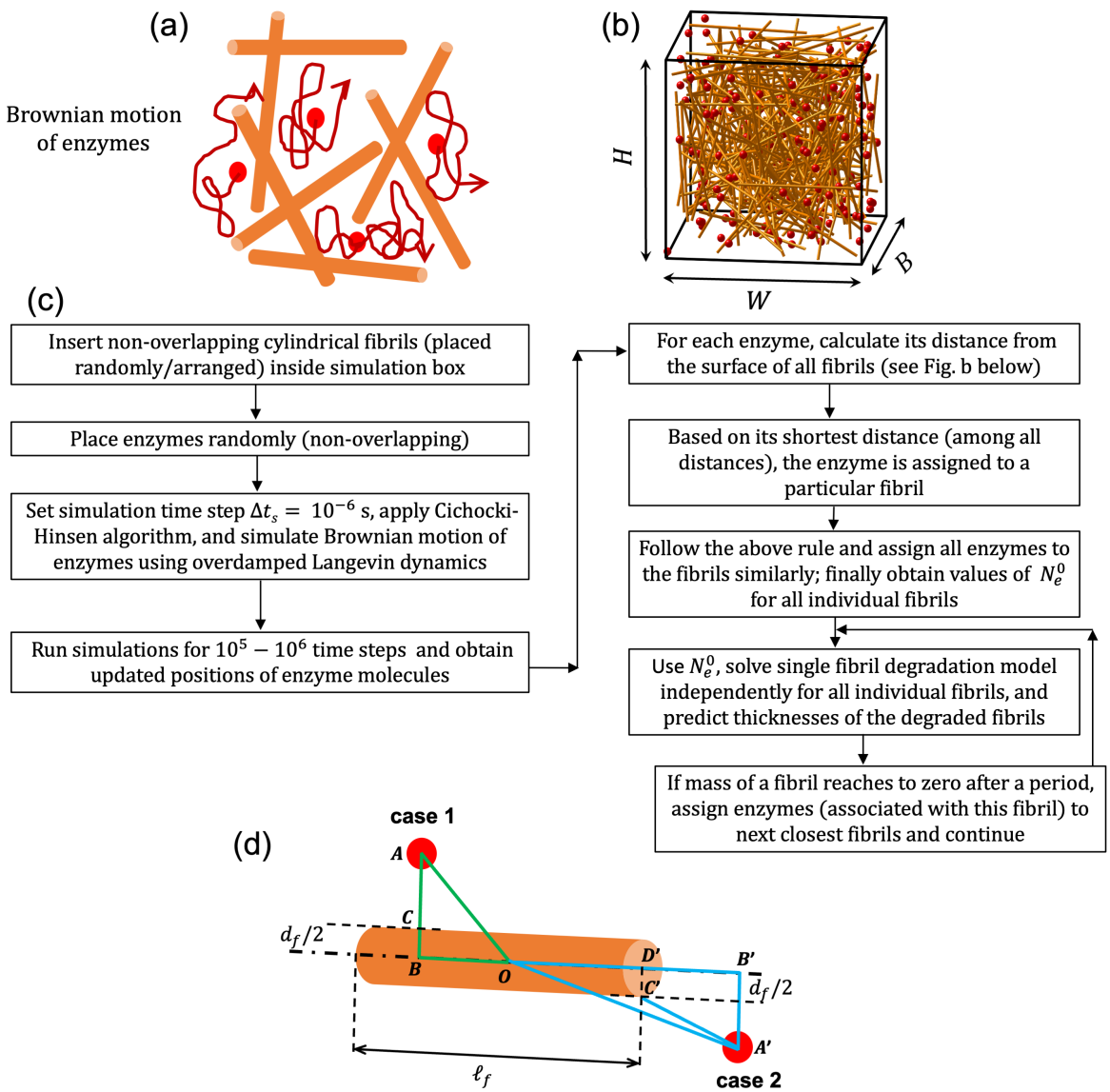

Figure 2: Brownian dynamics and hybrid simulation. (a) Schematic of the Brownian motion of enzymes inside the pores. (b) Configuration of the Brownian dynamics simulation where the cylinders represent collagen fibrils and the red spheres represent the enzyme molecules (not to scale). (c) Flowchart of the hybrid modeling approach. (d) Schematic representing the distance of an enzyme from the surface of a fibril. Based on the position of the enzyme with respect to any fibril surface, two cases are possible. For case 1, the distance chosen is $AC = AB - d_f/2$. Otherwise, $A'C' = \sqrt{(B'D')^2 + (A'B' - d_f/2)^2}$ is the chosen distance for case 2, where $B'D' = \sqrt{(OA')^2 - (A'B')^2} - \ell_f/2$.

of enzymes in simulation volume is $(N_e^0)_{total} \sim 1500$.

We fixed the enzyme concentration and vary the collagen concentration, or equivalently, the fibril fraction ϕ_f. Here ϕ_f is the ratio of the volume of all fibrils to the volume of the simulation box. See section SI8 for more details on estimation of the fibril fraction ϕ_f from a collagen concentration. By varying fibril diameter d_f, fibril length ℓ_f and number of fibrils n_f, we vary ϕ_f in the range $0.003 - 0.03$, i.e. $0.3 - 3\%$ for organs such as brain, liver, kidney, etc.[59]. These three parameters, d_f, ℓ_f and n_f, are important factors to address different matrix microarchitectures. The orientation and curvature (or, crimping) of the fibrils can be other factors[12], however, we did not consider their roles in the present work.

2.3 Experimental methods

Following the experimental methodologies of Ranamukhaarachchi et al.[11], we used rat tail type I collagen to synthesize the collagen gels. To vary the microarchitecture of the gels, we used polyethylene glycol (PEG) as a macro-molecular crowding agent. After polymerization of collagen using PEG at 37°C, PEG was washed out of the gels by rinsing them with Dulbecco's Modified Eagle Medium (DMEM) solution. We then treated the gels with a bacterial collagenase. To characterize the microarchitectures of the gels pre- and post-degradation, we performed fast green staining and imaging using the confocal fluorescence microscopy and scanning electron microscopy. See section SI9 for more details of the experimental methods.

3 Results

3.1 Single fibril degradation

We first calibrate single fibril model and compare single fibril surface erosion model against previously published experiments of Flynn et al.[21]. In the absence of external loading, our model captured the experimental trend (Fig. 3a). See section SI10 for

more details. When the fibril is under external loading, perhaps the external tension increases the stability of the triple helices by increasing the energy barrier for enzymatic unwinding[29,60–64], which is different from the mechanism for an isolated triple helix under external tension[65,66]. Under low loading of $\sim$ 2 pN per tropocollagen monomer[21,62], a small increase in the energy barrier E_m for enzymatic unwinding by $\delta E_m = 0.013\, E_m$ explains the experimental trend satisfactorily (Fig. 3a). See section SI10 for the choice of $\delta E_m = 0.013\, E_m$. Overall, our model captured the experimental trends for a degrading fibril under different external loading conditions reasonably well.

In a surface erosion process, the degradability of a fibril must be proportional to the ratio N_e^0/A_f^0, where N_e^0 and $A_f^0 = (\pi\, d_f^0\, \ell_f)$ are the number of enzymes surrounding a fibril and the initial surface area of the fibril, respectively. For a fibril of fixed initial diameter d_f^0, an increase in N_e^0 increases the degradability (Fig. 3b). However, for a fixed value of N_e^0, the degradability decreases with the increase in d_f^0 (Fig. 3c). The quantity $(d_f^0 - d_f)/d_f^0$ represents the relative decrease in the diameter. Its smaller value represents less degradation and *vice versa*. We provided a few results (Fig. S2) on degradability and the ratio N_e^0/A_f^0 in section SI10. In summary, our model predictions captured the scaling related to a surface erosion process.

3.2 Degradation of collagen matrices

Having established that the single fibril model captures experimentally observed degradation rates (Fig. 3a), we next focused on degradation of collagen fibrils in matrices. Before addressing matrix degradation, we define two important dependent parameters: the initial volume fraction of fibrils as $\phi_f = \left(n_f\, \frac{\pi}{4}\, \sum_i ((d_f^0)^2\, \ell_f)_i\right)/\text{vol.}^{\text{box}}$, and the initial total surface area (scaled) of fibrils as $(A_f^0)_{total} = \left(n_f\, \pi\, \sum_i (d_f^0\, \ell_f)_i\right)/l_p^2$.

Degradation of matrices with uniform fibrils

We first considered uniform fibrils of same initial diameter d_f^0 and length ℓ_f, and investigated the effect of the number of fibrils n_f, d_f^0, and ℓ_f on degradation. Using

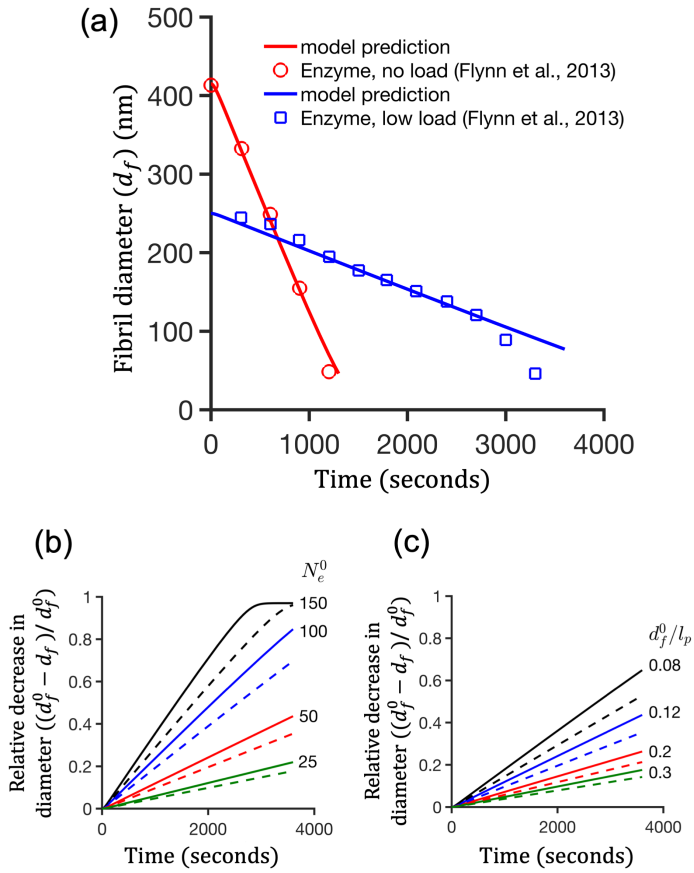

Figure 3: Degradation of single fibril. (a) Validation of the single fibril model with the experimental findings of Flynn et al.[21]. Relative decrease of fibril diameter $(d_f^0 - d_f)/d_f^0$ (or, the extent of degradation) with time for two cases: (b) fixed initial fibril diameter $d_f^0/l_p = 0.12$ and varying number of enzymes surrounding a fibril (N_e^0); (c) Varying d_f^0/l_p and fixed $N_e^0 = 50$. Here $l_p = 1$ µm is a nominal length scale. The length of the fibril is $\ell_f/l_p = 2$ in (b) and (c). The solid and dashed curves in (b) and (c) correspond to $k_+^c = 0.583$ s^{-1}[67] and 0.472 s^{-1}[68], respectively.

the hybrid approach described in Fig. 2b,c, we counted the number of enzymes N_e^0 surrounding every single fibril (Fig. 4a). We used this count of the number of enzymes to obtain a probability density function (PDF) of N_e^0 for a given matrix (Fig. 4b).

We observed that the enzyme distribution was not uniform across the fibrils in a matrix (Fig. 4a,b), suggesting that the organization of the collagen fibrils was a major determinant of the enzyme distribution. There are a few factors that can result in this non-uniform distribution of enzymes around fibrils. First, the cylindrical geometry of fibrils can result in an anisotropy of the diffusive motion of enzymes[69,70]. Even if the cylindrical geometries of the fibrils are taken into account, for enzyme distributions in a matrix to be nearly uniform, fibrils should be organized in an equidistant manner with parallel alignment. This organization ensures a uniform pore size around cylindrical fibrils and can result in nearly uniform enzyme distribution (see SI Fig. S3). However, the random placement and random orientation of fibrils induces a non-uniform distribution of pore sizes. These factors together can result in a non-uniform enzyme distribution in a fibrillar matrix. Our simulations show that this finding of non-uniform distribution of enzymes holds for different values of fibril diameter, fibril length, and number of fibrils (Fig. 4e).

The enzyme distributions do not differ much between two matrices if we vary only d_f^0, fixing $\ell_f/l_p = 2$ and $n_f = 25$ (Fig. 4b). Using the values of the number of enzymes in Fig. 4a, we solved the single fibril model for each of the individual fibrils and calculated the diameters of the fibrils (Fig. 4c). As expected, each fibril degrades to a different extent because of the difference in the number of enzymes surrounding it. Using these single fibril data, we obtained the PDF of the relative decrease in the diameter of the fibril $(d_f^0 - d_f)/d_f^0$ (Fig. 4d). Thus, we find that although the initial fibril diameter is uniform, the degraded fibrils have a distribution of diameters because of the non-uniform enzyme distribution.

We next investigated the effect of the number of fibrils n_f on the extent of degradation. From our simulations, we find that the enzyme distribution is a strong function of n_f (Fig. 4e). For a fixed value of $(N_e^0)_{total}$, we can expect a decrease in the average

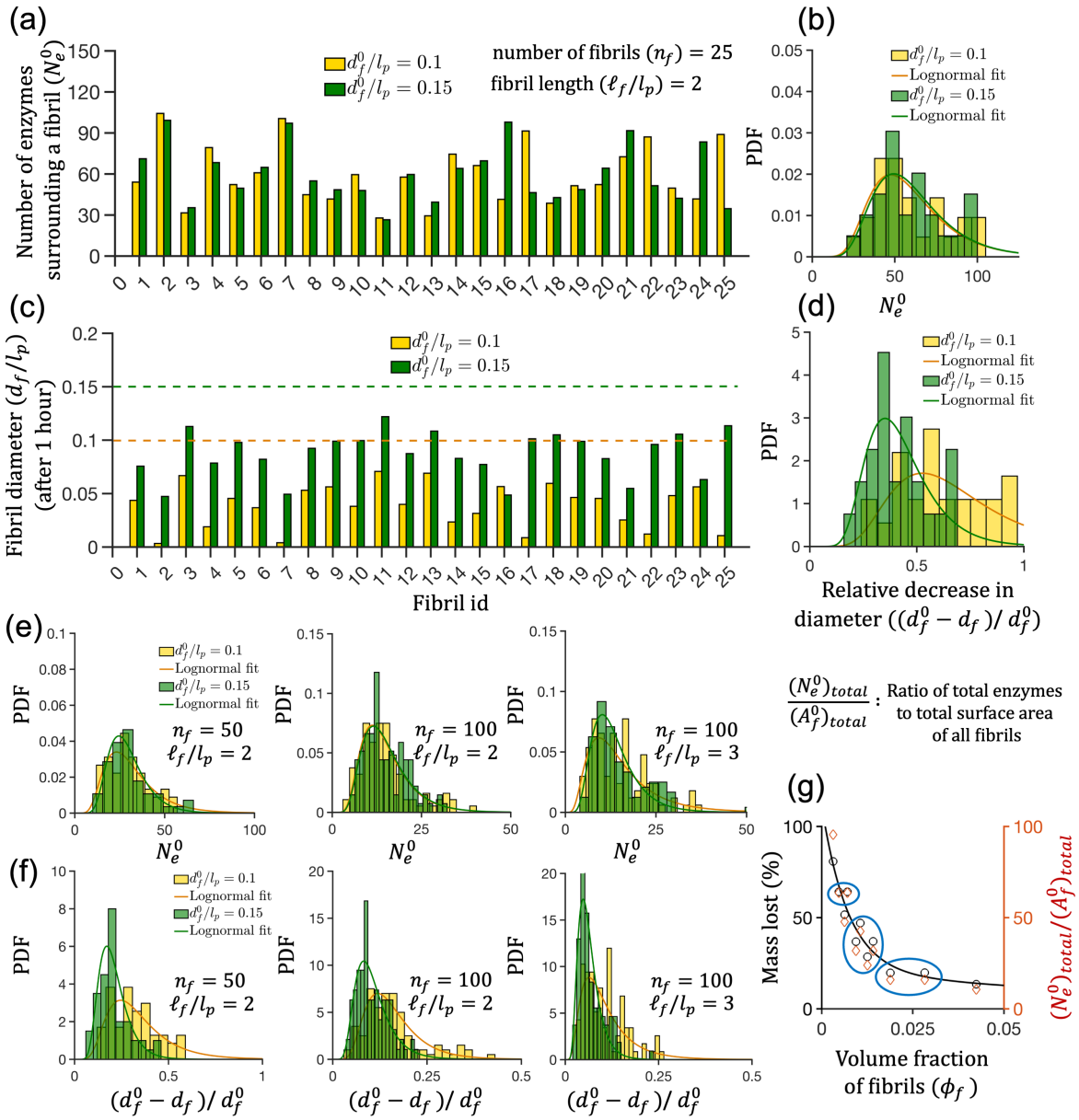

Figure 4: Degradation of collagen matrices. (a) The values of the number of enzymes N_e^0 surrounding the individual fibrils in a matrix for two different matrices of same fibril length ℓ_f and number of fibrils n_f, but for two different values of initial fibril diameter $d_f^0/l_p = 0.1$ and 0.15. (b) The probability density function (PDF) of N_e^0 generated using the data in (a). (c) The predicted diameters of the fibrils after 1 hour of degradation by enzymes for the cases in (a). (d) The PDFs representing the relative decrease in diameter $(d_f^0 - d_f)/d_f^0$ for the data shown in (c). Panels (e) and (f) represent PDFs of N_e^0 and $(d_f^0 - d_f)/d_f^0$ for different values of d_f^0, n_f and ℓ_f. (g) The percentage of the mass lost (left ordinate) and the ratio $(N_e^0)_{total}/(A_f^0)_{total}$ (right ordinate) with the volume fraction of fibrils ϕ_f. The black curve in (g) represents a fit to the data points corresponding to the left ordinate. The data points inside the blue circles show non-monotonous trends of the mass lost and the ratio $(N_e^0)_{total}/(A_f^0)_{total}$ with respect to ϕ_f.

value of N_e^0 per fibril if n_f increases. When comparing two matrices of the same d_f^0 and ℓ_f, the matrix with higher number of fibrils degrades to a lesser extent than the matrix with fewer fibrils (Fig. 4d,f). We also find that an increase in d_f^0 and ℓ_f decreases the degradability of the matrix for fixed values of n_f and $(N_e^0)_{total}$ (Fig. 4d,f) because of the decrease in the ratio $(N_e^0)_{total}/(A_f^0)_{total}$.

Effect of matrix architecture on fibril degradation

Since we model the single fibril degradation as a surface erosion process, the extent of degradation for a matrix must be proportional to the ratio of the total number of enzymes to the total surface area of the fibrils $(N_e^0)_{total}/(A_f^0)_{total}$. The overall mass lost, defined as

$$\text{mass lost} = \frac{\left[\sum_{id=1}^{n_f} \frac{\pi}{4} (d_f^0)_{id}^2 \, \ell_f\right] - \left[\sum_{id=1}^{n_f} \frac{\pi}{4} (d_f)_{id}^2 \, \ell_f\right]}{\sum_{id=1}^{n_f} \frac{\pi}{4} (d_f^0)_{id}^2 \, \ell_f} \times 100\,, \tag{11}$$

represents a direct estimate of the matrix degradation. In matrices, we considered the lost volume of all fibrils even if a thin fibril is fully digested. We used Eqn 11 to obtain the total mass lost. This equation includes all fibril volumes whether fully digested or not. For all combinations of n_f, d_f^0 and ℓ_f, we find a direct correlation between the mass lost and the ratio $(N_e^0)_{total}/(A_f^0)_{total}$ (Fig. 4g) when they are plotted against the fibril fraction ϕ_f. However, the variation of the mass lost and $(N_e^0)_{total}/(A_f^0)_{total}$ with ϕ_f are not strictly monotonous (blue circles in Fig. 4g), although their trends appear to be monotonically decreasing as ϕ_f increases. The circled data points in Fig. 4g show that for the same enzyme concentration, different extent of degradation can occur between two matrices of same fibril fraction ϕ_f (equivalently, the same collagen concentration) and *vice versa*. This finding leads to the following question: does the difference in microarchitecture of two matrices of same ϕ impact the extent of degradation? We answer this question by conducting the following simulations.

We fix the value of ϕ_f and the enzyme concentration, and consider the matrices with

uniform fibrils. Without varying ℓ_f, different matrices of same ϕ_f can be generated by adjusting the values of n_f and d_f^0 (Fig. 5a). For example, as $\phi_f \propto n_f\,(d_f^0)^2$, a 50% decrease in d_f^0 can increase n_f up to 4 times, resulting in twice the increase of the surface area ($(A_f^0)_{total} \propto n_f\, d_f^0$). For the case of constant ϕ_f and smaller d_f^0, n_f increases and shifts the enzyme distribution towards the left (Fig. 5b). Simulations show that a matrix composed of thinner fibrils degrades less than that a matrix composed of thicker fibrils (Fig. 5c). This is an unexpected result and counterintuitive to what we might expect from a single fibril model. In the single fibril degradation model, a thinner fibril degrades more than a thicker fibril if the enzyme concentration is the same (Fig. 3c) because of lesser surface area of a thinner fibril available to larger number of enzymes. In contrast, in a three-dimensional, randomly oriented and randomly placed fibril network, multiple factors affect the enzyme distribution as discussed previously. Thus, this finding highlights the importance of incorporating the three-dimensional spatial considerations including diffusion of enzymes and matrix microarchitectures into the model. The results in Fig. 5d-f show how the number of fibrils changes for different sets of (d_f^0, ℓ_f) when ϕ_f is fixed, which directly influences the ratio $(N_e^0)_{total}/(A_f^0)_{total}$, and the overall mass lost. In summary, our simulations predict that for the same enzyme concentration, uniform fibril diameter, and the same fibril fraction ϕ_f, a matrix with thicker fibrils can degrade more than that with thinner fibrils (Figs. 5d-f).

To compare this model prediction on matrix degradability, we performed *in vitro* experiments with synthetic collagen gels and investigated their degradability.

3.3 Experiments reveal that matrix microarchitecture governs degradability

Ranamukhaarachchi et al.[11] previously showed that the microarchitecture of a collagen gel can be modulated using polyethylene glycol (PEG) as a macro-molecular crowding (MMC) agent. They also reported that the degradability of the gels varies with the matrix microarchitecture. Using this background, to test our model predic-

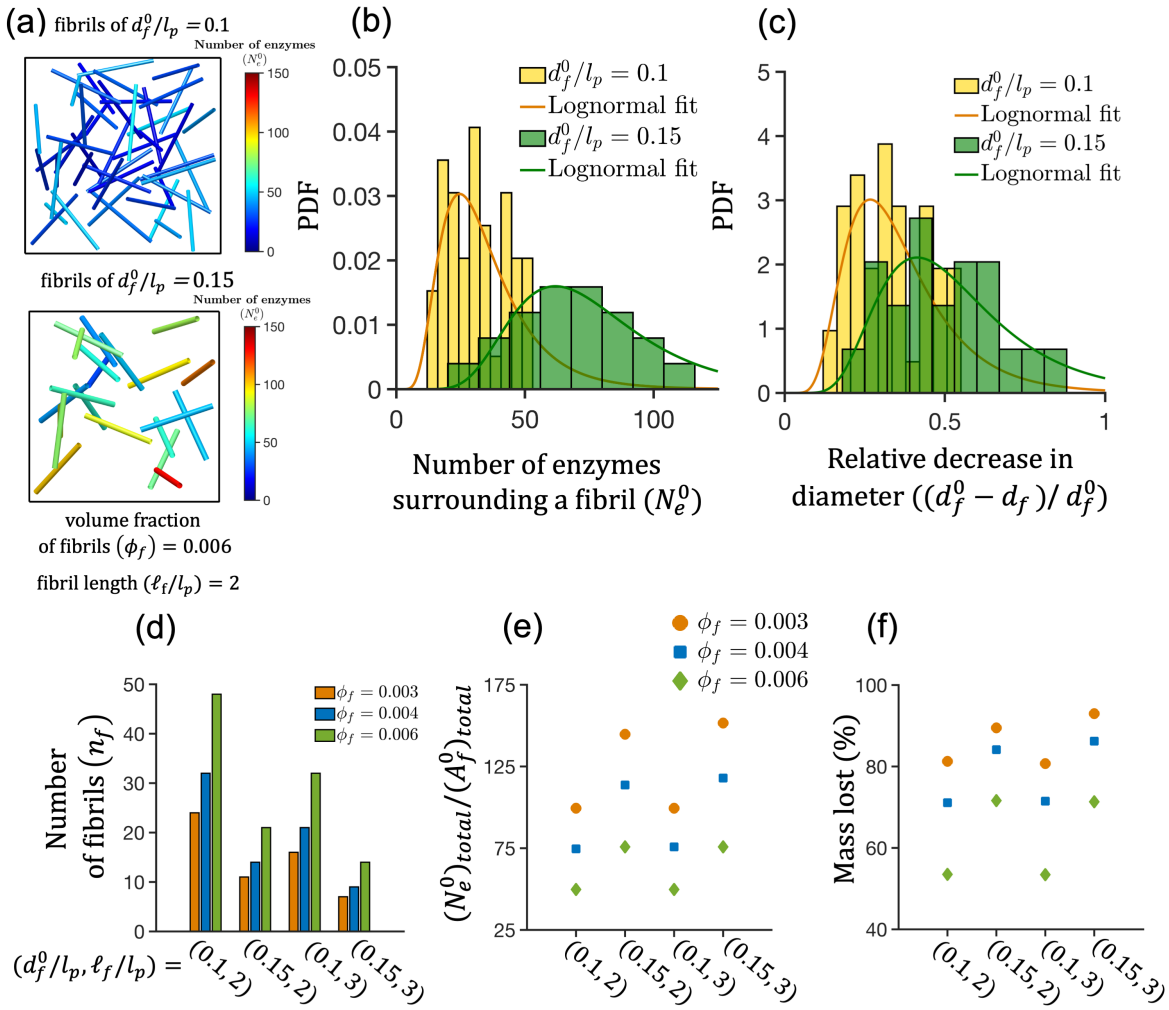

Figure 5: Matrix with thicker fibrils degrades more than that with thinner fibrils. (a) The initial configurations of two matrices having the same fibril fraction $\phi_f = 0.006$. The color bars in (a) represent the number of enzymes (N_e^0) surrounding the fibrils. For the configuration in (a), the PDF of enzyme distribution N_e^0 (b) and the PDF of the extent of degradation of fibrils $(d_f^0 - d_f)/d_f^0$ (c). For matrices having different ϕ_f, the first (d), second (e) and third (f) panels report the number of fibrils in matrices, $(N_e^0)_{total}/(A_f^0)_{total}$ and the percentage mass lost (overall degradation of matrices), respectively. All results correspond to the total number of enzymes $(N_e^0)_{total} = 1500$ and time 60 minutes.

tions, we prepared collagen gels with two different microarchitectures from the same collagen concentration. We used 2.5 mg/ml collagen (final concentration) and two different MMC concentrations: 2 mg/mL PEG designated as P2 and 8 mg/mL PEG denoted as P8 (Fig. 6a). We used a bacterial collagenase concentration of 2.5 µg/mL (final concentration) to perform degradation experiments. Using fast green staining images and scanning electron microscopy (SEM), we quantified the fibril length and thickness distributions respectively before and after degradation. We denote the gels post-degradation as P2x and P8x.

Fig. 6b shows the fast green stained images, and the length distributions for P2/P2x (Fig. 6c) and P8/P8x (Fig. 6d). The mean length of the fibrils in P8 ($\sim 3 \pm 0.2$ µm) is slightly smaller than that of P2 ($\sim 3.3 \pm 0.4$ µm). From Fig. 6b, it is obvious that P2 degrades more than P8 as larger pores are present in P2x. However, there is no significant change in the length distributions before and after degradation in both P2/P2x and P8/P8x (Fig. 6c,d); the decrease in the mean length post-degradation is less than $\sim 8\%$. Hence the assumption of treating the fibril length ℓ_f as a constant in our model is supported by the experimental findings. The green stained images (Fig. 6b) reveal that the number of fibrils is higher in P8 than that in P2 (through visualization).

The SEM images (Fig. 6e) and the histograms of the fibril diameters (Fig. 6f,g) show that the fibrils are thicker in P2 than in P8. The mean diameter of the fibrils in P8 ($\sim 0.09 \pm 0.02$ µm) is $\sim$ 25-30% smaller than that of P2 ($\sim 0.13 \pm 0.03$ µm). After degradation, the decrease in the diameter occurs in both P2x and P8x (Fig. 6f,g). We performed statistical comparisons of the distributions by log normal fits (see section SI11). We did not find significant differences in length distributions, but there are differences in the diameter distributions. Quantification of the diameters of the fibrils show that P2 (Fig. 6f) degrades more than P8 (Fig. 6g). The decrease in the mean diameter is $\sim 30 - 40\%$ in P2x and $\sim 15\%$ in P8x. Thus, experiments validate our model predictions that a matrix with thicker fibrils can degrade more than one with thinner fibrils for the same collagen and collagenase concentrations.

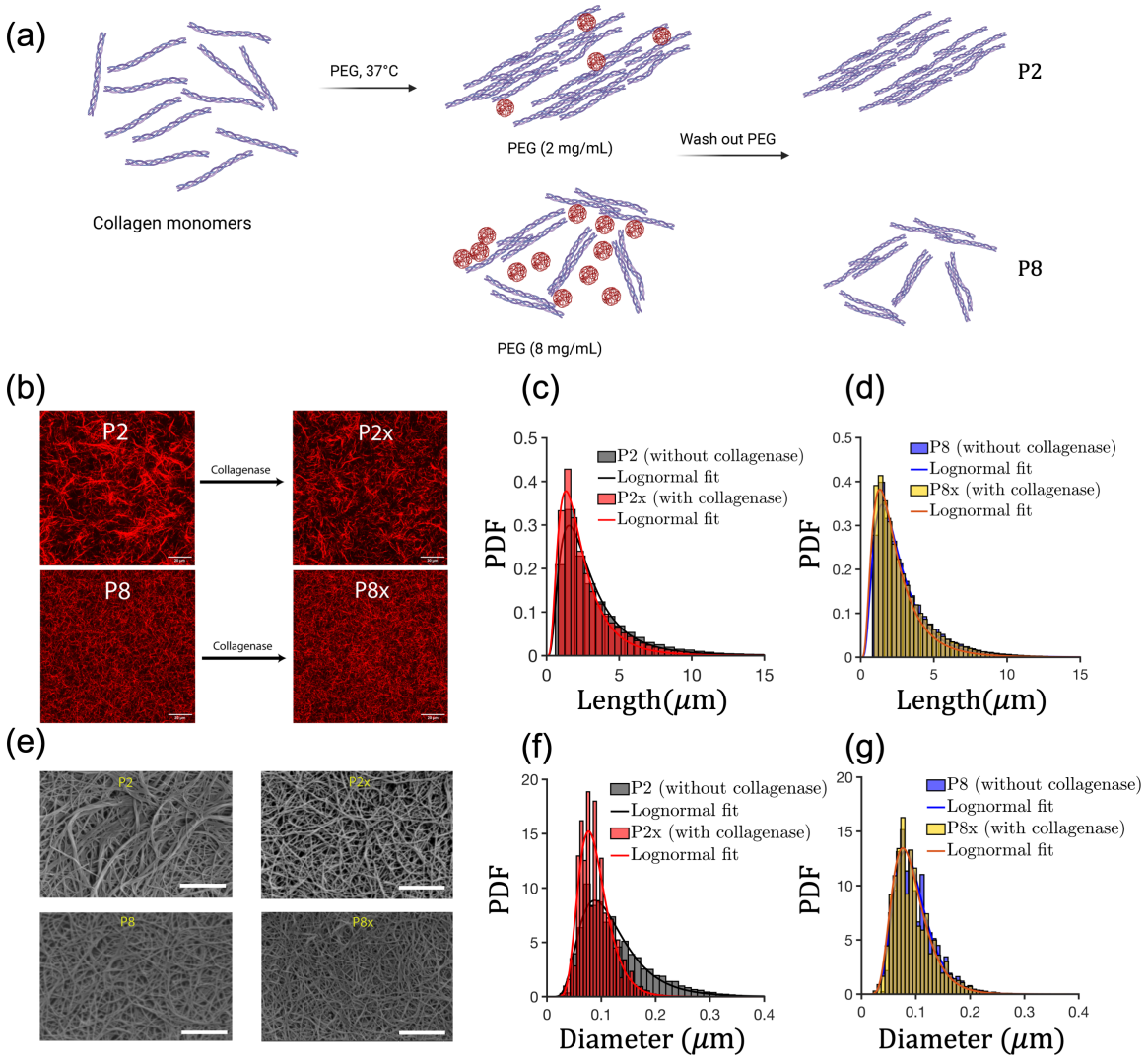

Figure 6: Experimental findings. (a) Preparation of collagen gels. (b) The fast green stained images of the gels (scale bar 20 μm). The length distributions of (c) P2/P2x and (d) P8/P8x before and after treatment with collagenase from the green stained images. (e) The SEM images of P2/P2x and P8/P8x (scale bar 2 μm). The histograms of fibril diameters for (f) P2/P2x and (g) P8/P8x.

Model predictions for matrices with non-uniform fibrils highlight the role of microarchitecture in degradation

To further reinforce the role of matrix microarchitecture, we note that the significant differences between the microarchitectures of P2 and P8 are primarily due to the number of fibrils and fibril diameter. In P2, there are less number of fibrils and the fibrils are thicker. However, in P8, there are higher number of fibrils but the fibrils are thinner, compared to P2 (Fig. 6). Our model predicts higher degradability of a matrix with thicker fibrils than that with thinner fibrils (Figs. 5). Thus, we can qualitatively explain why the matrix with the P2 architecture degrades more than the P8 architecture. However, our simulations in Fig. 5 are for fibrils of uniform initial diameter. Because the experimentally synthesized matrices had fibrils with a distribution of diameters, we next simulated the degradation of fibrils in matrices of experimentally-inspired fibril diameter distributions.

We generated the fibrils whose diameters matched the experimentally observed diameters of P2 and P8 (Fig. S5 and Fig. S6 in section SI11 for more details). In any matrix (whether P2 or P8), we set the length of the fibrils the same. As the mean length of P8 is approximately 8–10% smaller than that of P2 in experimental findings, we set the mean fibril length of P8 10 % smaller than that of P2 in simulations. We used a fibril fraction of $\phi_f = 0.007$ in both cases as this value is close to the collagen concentration used in the experiments. As a result, in these newly generated matrices, the number of fibrils is higher for P8 ($n_f \sim 75$) than that in P2 ($n_f \sim 40$) for the same fibril fraction ϕ_f. We compared the outcomes of degradation in these conditions as shown in Fig. 7. The microarchitectures are different for P2 and P8 (Fig. 7a,b) in terms of the number of fibrils and the diameters. As a result, the enzyme distribution for P8 shifts to the left due to larger number of fibrils (Fig. 7c) and implies less number of enzymes per fibril. The diameter distributions (in the range 0.03-0.2 µm) of P2 and P8 before and after degradation (Fig. 7d,e) and the overall mass lost (Fig. 7f) indicate that P2 degrades more than P8 for the same collagen and enzyme concentrations, in agreement with

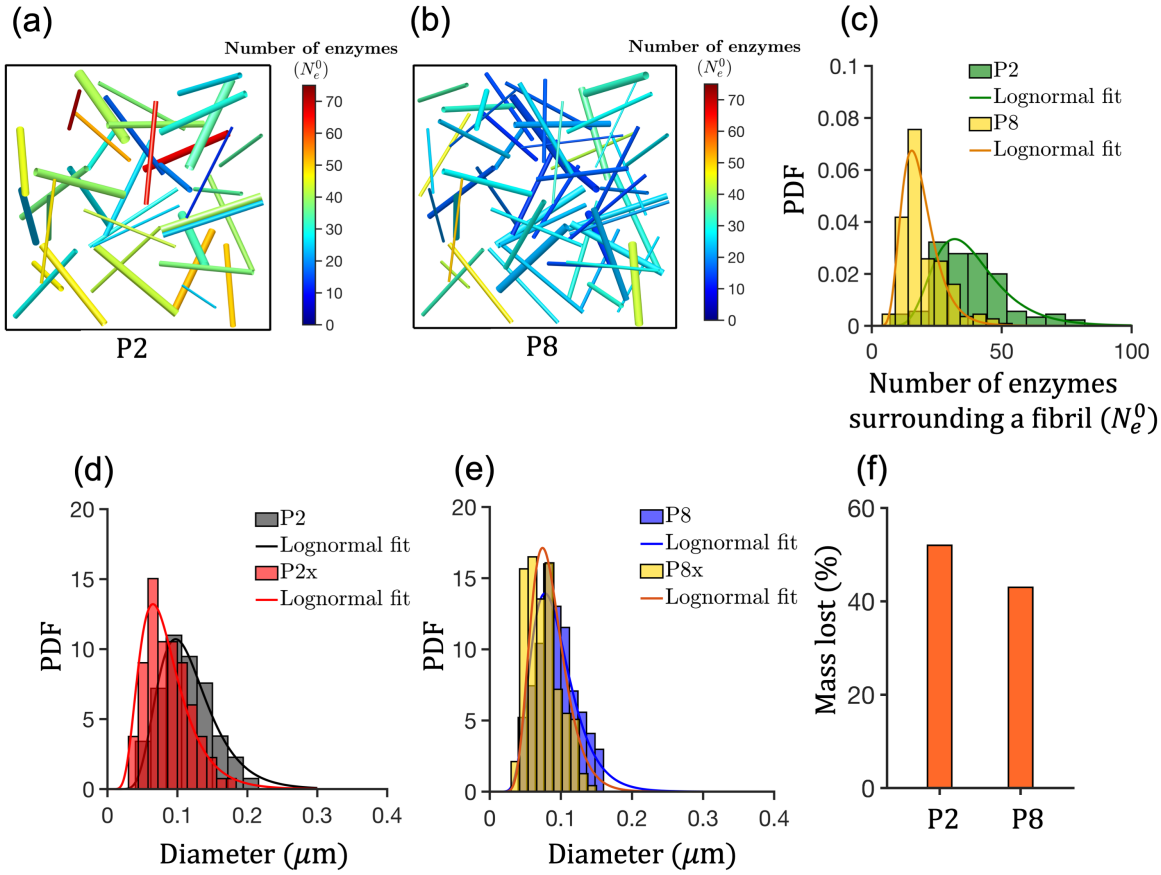

Figure 7: Simulations of matrices with non-uniform fibrils predict that P2 degrades higher than P8. The initial configurations of two matrices, P2 (a) and P8 (b), with the same fibril fraction $\phi_f = 0.007$. The color bars in (a) and (b) represent the number of enzymes (N_e^0) surrounding the fibrils. For the configuration in (a) and (b), the PDF of the enzyme distributions N_e^0 (c), the PDF of the diameters of the fibrils for P2/P2x (d) and P8/P8x (e), and the overall mass lost (f). The results correspond to the total number of enzymes $(N_e^0)_{total} = 1500$ and time 60 minutes.

experiments (Fig. 6e,f). Our simulation results using non-uniform fibril diameter only reinforce our model predictions that the matrices of the same collagen concentration can have very different microarchitectures and the matrices can degrade differently under the same collagenase concentration. In summary, our study reveals that matrix microarchitecture plays an important role in degradation of collagen matrices.

4 Discussion

In this study, using a combination of modeling and experiments, we investigated the collagenolytic degradation of collagen matrices. Unraveling the connection between the matrix microarchitecture and degradation is important to design biomaterials and understand ECM remodeling at cellular length scale. Previous models are either continuum or discrete, and thus, they predict either overall rate of degradation or degradation at the nanoscale[14,15,17,19]. The model and framework we developed in this work to investigate the collagen matrix microarchitecture and matrix degradation is novel in the sense that it addresses the connection between the nanoscale degradation and the microscale microarchitecture.

The single fibril component of our model shows the capability to capture experimental trends under different loading conditions. Furthermore, the integration of multiscale model components shows that matrix microarchitecture is a strong determinant of matrix degradability. This relationship emerges because the fibrillar network causes the enzyme distribution in a matrix to be non-uniform, and this enzyme distribution leads to fibrils of distributed diameters even if the fibrils are initially uniform in size. This explains how matrices of the same collagen concentration but different microarchitectures can degrade differently under the same collagenase concentration. These findings are backed by *in vitro* experiments with collagen gels of different microarchitectures.

However, our model has also some drawbacks. The lattice-based single fibril model has a limitation to predict the spatial variations in the size and shape of a degrading fibril. In our simulations, the fibrils are non-stretchable, and we did not explicitly con-

sider explicitly the potential energy based attractive interactions among the fibrils and enzymes. At present, it is difficult to state *a priori* whether the potential interactions can affect the temporal evolution of the enzyme distribution which merits further attention. One of the limitations of our current simulation strategy is that we modelled collagen fibrils as rigid rods, therefore it is not possible to simulate single fibril degradation under tension using the current simulation framework. One possible way to simulate soft fibrils under tension can be using molecular dynamics simulations. Many researchers performed molecular dynamics at the tropocollagen scale (for example, see Chang et al.[60]). While molecular dynamics simulations are outside the scope of the present work, we anticipate future advances in this area.

Another important opportunity would be predicting matrix degradation under different external stretching conditions. Some experimental observations[71,72] reported that the degradation rate of a matrix decreases and then increases with an increase in strain, leading to a V-shape profile for degradation rates as a function of loading. Our model is currently able to predict matrix degradation under no external stretching conditions. The presence of fibril connectivity and crosslinks may change the force distribution among the degrading fibrils under tension. Future enhancements to our simulation framework include simulations of soft fibrils with fibril connectivity and crosslinks. Furthermore, the current hybrid model does not consider fibril orientation, the effect of crosslinking and crimping of fibrils. We speculate that the crimping induced curvature and orientation may influence enzyme distribution and degradability. These topics merit more attention and form a part of future work.

In summary, our single fibril model and hybrid modeling framework effectively capture multi-scale effects to predict the degradation of three-dimensional matrices with different microarchitectures. Although relatively simple, this framework sheds light on how collagen matrix degradability is tuned by matrix microarchitecture. Further model developments can also include additional vulnerable sites for making it specific to the bacterial collagenase[29]. Such modifications will reflect in the changes of the rate constants and initial number of vulnerable sites. However, the mechanism of enzyme

induced permanent unwinding will likely remain the same.

This work has important implications for a number of fields, including matrix biology, cell migration, and biomaterials. A recent work[13] showed that matrix degradability can translate into differences in stress relaxation that can be sensed by cells through effects on cell-matrix adhesions. Perhaps related to this phenomenon, another work[73] showed that cell invasiveness is upregulated for breast cancer cells inside collagen networks comprised of thick fibrils, whereas the invasiveness decreased substantially for thin fibrils of similar pore diameter and elastic modulus. These observed differences in invasiveness may be linked to the differences in the degradability and resulting mechanical changes of thick and thin fibrillar architectures. An important future direction is to scale modeling efforts to decellularized ECM and tissues. In the field of biomaterial design, synthetic matrices developed so far focus on recapitulate the biochemical and mechanical features of the ECM. Controlling the degradability by mimicking native collagen architectures[11,12,74] could offer valuable insights into cellular function.

Conflicts of interest

There are no conflicts to declare.

Acknowledgements

This work was supported by a National Science Foundation grant DMS-1953469, American Cancer Society Research Scholar Grant RSG-21-033-01-CSM to S.I.F., the National Cancer Institute U54CA274502, a Prebys Research Heroes Grant to S.I.F. P.R. and S.I.F were also supported by the Wu Tsai Human Performance Alliance and the Joe and Clara Tsai Foundation. We would like to thank the UC San Diego School of Medicine Microscopy Core, which is supported by the National Institute of Neurological Disorders and Stroke grant NINDS P30NS047101.

References

[1] Wohlgemuth R, Brashear S, Smith L. Alignment, cross linking, and beyond: a collagen architect's guide to the skeletal muscle extracellular matrix. American J Physiology-Cell Physiology. 2023;325:C1017-30.

[2] Gupta V, Vaishnavi V, Arrieta-Ortiz M, PS A, KM J, Jeyasankar S, et al. 3D Hydrogel Culture System Recapitulates Key Tuberculosis Phenotypes and Demonstrates Pyrazinamide Efficacy. Adv Healthcare Mater. 2024:2304299.

[3] Wynn T, Ramalingam T. Mechanisms of fibrosis: therapeutic translation for fibrotic disease. Nat Medicine. 2012;18:1028-40.

[4] McKleroy W, Lee T, Atabai K. Always cleave up your mess: targeting collagen degradation to treat tissue fibrosis. American J Physiology-Lung Cellular and Molecular Physiology. 2013;304:L709-21.

[5] Huang L, Haylor J, Hau Z, Jones R, Vickers M, Wagner B, et al. Transglutaminase inhibition ameliorates experimental diabetic nephropathy. Kidney International. 2009;76:383-94.

[6] Philp C, Siebeke I, Clements D, Miller S, Habgood A, John A, et al. Extracellular matrix cross-linking enhances fibroblast growth and protects against matrix proteolysis in lung fibrosis. American J Respiratory cell and Molecular Biology. 2018;58:594-603.

[7] Nebuloni M, Albarello L, Andolfo A, Magagnotti C, et al. Insight on colorectal carcinoma infiltration by studying perilesional extracellular matrix. Sci Rep. 2016;6:22522.

[8] Liotta L, Tryggvason K, Garbisa S, Hart I, Foltz C, Shafie S. Metastatic potential correlates with enzymatic degradation of basement membrane collagen. Nature. 1980;284:67-8.

[9] Winkler J, Abisoye-Ogunniyan A, Metcalf K, Werb Z. Concepts of extracellular matrix remodelling in tumour progression and metastasis. Nat Commun. 2020;11:5120.

[10] Dewavrin J, Hamzavi N, Shim V, Raghunath M. Tuning the architecture of three-dimensional collagen hydrogels by physiological macromolecular crowding. Acta Biomat. 2014;10:4351-9.

[11] Ranamukhaarachchi S, Modi R, Han A, Velez D, Kumar A, Engler A, et al. Macromolecular crowding tunes 3D collagen architecture and cell morphogenesis. Biomaterials Sci. 2019;7(2).

[12] Ashworth J, Cox T. The importance of 3D fibre architecture in cancer and implications for biomaterial model design. Nat Rev Cancer. 2024;24:461-79.

[13] Narasimhan B, Fraley S. Degradability tunes ECM stress relaxation and cellular mechanics. BioRxiv. 2024:2024-07.

[14] Tzafriri A, Bercovier M, Parnas H. Reaction diffusion model of the enzymatic erosion of insoluble fibrillar matrices. Biophysical journal. 2002;83(2).

[15] Metzmacher I, Radu F, Bause M, Knabner P, Friess W. A model describing the effect of enzymatic degradation on drug release from collagen minirods. Euro J Pharma Biopharma. 2007;67(2):349-60.

[16] Ray N, van Noorden T, Radu F, Friess W, Knabner P. Drug release from collagen matrices including an evolving microstructure. ZAMM-Journal of Applied Mathematics and Mechanics. 2013;93(10-11).

[17] Vuong A, Rauch A, Wall W. A biochemo-mechano coupled, computational model combining membrane transport and pericellular proteolysis in tissue mechanics. Proc Royal Soc A. 2017;473(2199).

[18] Saffarian S, Collier I, Marmer B, Elson E, Goldberg G. Interstitial collagenase is a Brownian ratchet driven by proteolysis of collagen. Science. 2004;306(5693).

[19] Sarkar S, Marmer B, Goldberg G, Neuman K. Single-molecule tracking of collagenase on native type I collagen fibrils reveals degradation mechanism. Current Biol. 2012;22(12).

[20] Bhole A, Flynn B, Liles M, Saeidi N, Dimarzio C, Ruberti J. Mechanical strain enhances survivability of collagen micronetworks in the presence of collagenase: implications for load-bearing matrix growth and stability. Phil Tran Roy Soc A: Mathematical, Physical and Engineering Sciences. 2009;367:3339-62.

[21] Flynn B, Tilburey G, Ruberti J. Highly sensitive single-fibril erosion assay demonstrates mechanochemical switch in native collagen fibrils. BMMB. 2013;12:291-300.

[22] Staunton J, Vieira W, Fung K, Lake R, Devine A, Tanner K. Mechanical properties of the tumor stromal microenvironment probed in vitro and ex vivo by in situ-calibrated optical trap-based active microrheology. Cellular and Molecular Bioengineering. 2016;9:398-417.

[23] Seo B, Chen X, Ling L, Song Y, Shimpi A, Choi S, et al. Collagen microarchitecture mechanically controls myofibroblast differentiation. Proc Nat Acad Sci. 2020;117:11387-98.

[24] Daly A, Riley L, Segura T, Burdick J. Hydrogel microparticles for biomedical applications. Nat Rev Mat. 2020;5:20-43.

[25] Kim S, Min S, Choi Y, Jo S, Jung J, Han K, et al. Tissue extracellular matrix hydrogels as alternatives to Matrigel for culturing gastrointestinal organoids. Nat Commun. 2022;13:1692.

[26] Orgel J, Irving T, Miller A, Wess T. Microfibrillar structure of type I collagen in situ. Proc Nat Acad Sci. 2006;103(24).

[27] Buehler M. Nanomechanics of collagen fibrils under varying cross-link densities: atomistic and continuum studies. JMBBM. 2008;1(1).

[28] Marino M, Vairo G. Stress and strain localization in stretched collagenous tissues via a multiscale modelling approach. Computer Methods in Biomechanics and Biomedical Engineering. 2014;17:11-30.

[29] Saini K, Cho S, Dooling L, Discher D. Tension in fibrils suppresses their enzymatic degradation–A molecular mechanism for 'use it or lose it'. Matrix Biol. 2020;85.

[30] Chung L, Dinakarpandian D, Yoshida N, Lauer-Fields J, Fields G, Visse R, et al. Collagenase unwinds triple-helical collagen prior to peptide bond hydrolysis. EMBO. 2004;23:3020-30.

[31] Nagase H, Visse R. Triple helicase activity and the structural basis of collagenolysis. In: Extracellular Matrix Degradation. Springer; 2011. p. 95-122.

[32] Okada T, Hayashi T, Ikada Y. Degradation of collagen suture in vitro and in vivo. Biomaterials. 1992;13(7).

[33] Perumal S, Antipova O, Orgel J. Collagen fibril architecture, domain organization, and triple-helical conformation govern its proteolysis. Proc Nat Acad Sci. 2008;105(8).

[34] Tyn M, Gusek T. Prediction of diffusion coefficients of proteins. Biotech and Bioengg. 1990;35(4).

[35] Han S, Makareeva E, Kuznetsova N, DeRidder A, Sutter M, Losert W, et al. Molecular mechanism of type I collagen homotrimer resistance to mammalian collagenases. J Biol Chem. 2010;285(29).

[36] Visse R, Nagase H. Matrix metalloproteinases and tissue inhibitors of metalloproteinases: structure, function, and biochemistry. Circulation Res. 2003;92(8).

[37] Iyer S, Visse R, Nagase H, Acharya K. Crystal structure of an active form of human MMP-1. J Mol Biol. 2006;362(1).

[38] Manka S, Carafoli F, Visse R, Bihan D, Raynal N, Farndale R, et al. Structural insights into triple-helical collagen cleavage by matrix metalloproteinase 1. Proc Nat Acad Sci. 2012;109(31).

[39] Adamczyk Z, Senger B, Voegel J, Schaaf P. Irreversible adsorption/deposition kinetics: A generalized approach. J Chem Phys. 1999;110(6).

[40] Fang F, Satulovsky J, Szleifer I. Kinetics of protein adsorption and desorption on surfaces with grafted polymers. Biophys J. 2005;89(3).

[41] Nerenberg P, Salsas-Escat R, Stultz C. Do collagenases unwind triple-helical collagen before peptide bond hydrolysis? Reinterpreting experimental observations with mathematical models. Proteins. 2008;70(4).

[42] Eyring H. The activated complex and the absolute rate of chemical reactions. Chem Rev. 1935;17(1).

[43] Eyring H. Viscosity, plasticity, and diffusion as examples of absolute reaction rates. J Chem Phys. 1936;4(4).

[44] Tobolsky A, Eyring H. Mechanical properties of polymeric materials. J Chem Phys. 1943;11(3).

[45] Eckhard U, Schönauer E, Nüss D, Brandstetter H. Structure of collagenase G reveals a chew-and-digest mechanism of bacterial collagenolysis. Nat Struct Mol Biol. 2011;18:1109-14.

[46] Adjari A, Brochard-Wyart F, de Gennes P, Leibler L, Viovy J, Rubinstein M. Slippage of an entangled polymer melt on a grafted surface. Physica A: Statistical Mechanics and its Applications. 1994;204:17-39.

[47] Sung W. Slippage of linear flows of entangled polymers on surfaces. Phys Rev E. 1995;51:5862.

[48] Glasstone S, Laidler K, Eyring H. The theory of rate processes: the kinetics of chemical reactions, viscosity, diffusion and electrochemical phenomena. McGrawHill Book, New York. 1941.

[49] Stuart D, Anderson O. Dependence of ultimate strength of glass under constant load on temperature, ambient atmosphere, and time. J American Ceramic Soc. 1953;36(12).

[50] Raphael E, De Gennes P. Rubber-rubber adhesion with connector molecules. J Phys Chem. 1992;96(10).

[51] Léger L, Creton C. Adhesion mechanisms at soft polymer interfaces. Phil Tran Roy Soc A. 2008;366(1869).

[52] Ermak D, McCammon J. Brownian dynamics with hydrodynamic interactions. J Chem Phys. 1978;69(4).

[53] Islam M, Tudryn G, Picu C. Microstructure modeling of random composites with cylindrical inclusions having high volume fraction and broad aspect ratio distribution. Compt Mat Sci. 2016;125:309-18.

[54] Ayad A. Generate fiber. wwwmathworkscom/matlabcentral/fileexchange/73392-generate-fiber. 2024.

[55] Cichocki B, Hinsen K. Dynamic computer simulation of concentrated hard sphere suspensions: I. Simulation technique and mean square displacement data. Physica A. 1990;166(3).

[56] Smith S, Grima R. Fast simulation of Brownian dynamics in a crowded environment. J Chem Phys. 2017;146(2).

[57] Smith S, Cianci C, Grima R. Macromolecular crowding directs the motion of small molecules inside cells. J Roy Soc Interface. 2017;14(131).

[58] Schultz K, Anseth K. Monitoring degradation of matrix metalloproteinases-cleavable PEG hydrogels via multiple particle tracking microrheology. Soft Matter. 2013;9(5).

[59] Tarnutzer K, Siva Sankar D, Dengjel J, Ewald C. Collagen constitutes about 12% in females and 17% in males of the total protein in mice. Sci Rep. 2023;13:4490.

[60] Chang S, Flynn B, Ruberti J, Buehler M. Molecular mechanism of force induced stabilization of collagen against enzymatic breakdown. Biomaterials. 2012;33:3852-9.

[61] Chang S, Buehler M. Molecular biomechanics of collagen molecules. Materials Today. 2014;17:70-6.

[62] Tonge T, Ruberti J, Nguyen T. Micromechanical modeling study of mechanical inhibition of enzymatic degradation of collagen tissues. Biophysical J. 2015;109:2689-700.

[63] Alves C, Araújo A, Oliveira C, Imsirovic J, Bartolák-Suki E, Andrade J, et al. Homeostatic maintenance via degradation and repair of elastic fibers under tension. Sci Rep. 2016;6(1):27474.

[64] Topol H, Demirkoparan H, Pence T. Fibrillar collagen: A review of the mechanical modeling of strain-mediated enzymatic turnover. Applied Mech Rev. 2021;73:050802.

[65] Adhikari A, Chai J, Dunn A. Mechanical load induces a 100-fold increase in the rate of collagen proteolysis by MMP-1. J American Chem Soc. 2011;100:513a.

[66] Adhikari A, Glassey E, Dunn A. Conformational dynamics accompanying the proteolytic degradation of trimeric collagen I by collagenases. J American Chem Soc. 2012;134:13259-65.

[67] Mallya S, Mookhtiar K, Van Wart H. Kinetics of hydrolysis of type I, II, and III collagens by the class I and II Clostridium histolyticum collagenases. J Protein Chem. 1992;11.

[68] Welgus H, Jeffrey J, Stricklin G, Eisen A. The gelatinolytic activity of human skin fibroblast collagenase. J Biol Chem. 1982;257(19).

[69] Stylianopoulos T, Diop-Frimpong B, Munn L, Jain R. Diffusion anisotropy in collagen gels and tumors: the effect of fiber network orientation. Biophys J. 2010;99:3119-28.

[70] Chen P, Chen X, Hepfer R, Damon B, Shi C, Yao J, et al. A noninvasive fluorescence imaging-based platform measures 3D anisotropic extracellular diffusion. Nat Commun. 2021;12:1913.

[71] Huang C, Yannas I. Mechanochemical studies of enzymatic degradation of insoluble collagen fibers. J Biomed Mat Res. 1977;11(1):137-54.

[72] Yeganegi A, Whitehead K, de Castro B L, Richardson W. Mechanical strain modulates extracellular matrix degradation and byproducts in an isoform-specific manner. Biochimica et Biophysica Acta (BBA)-General Subjects. 2023;1867(3):130286.

[73] Sapudom J, Riedl P, Schricker M, Kroy K, Pompe T. Physical network regimes of 3D fibrillar collagen networks trigger invasive phenotypes of breast cancer cells. Biomaterials Advances. 2024;163:213961.

[74] Su H, Yang F, Fu R, Trinh B, Sun N, Liu J, et al. Collagenolysis-dependent DDR1 signalling dictates pancreatic cancer outcome. Nature. 2022;610(7931):366-72.

Data Availability Statement

Raw data supporting the findings of this study will be made available upon reasonable request. The entire codebase used in this work along with a readme file is available at https://github.com/RangamaniLabUCSD/Collagen_matrix_degradation.git .